RSC Advances

ROYAL SOCIETY OF CHEMISTRY

www.rsc.org/advances

Combustion Characterization and Modeling of Novel Nanoenergetic Composites of Co_3O_4/nAl

Vinay Kumar Patel[1], Jayant Raj Saurav[1], Keshab Gangopadhyay[2], Shubhra Gangopadhyay[2], Shantanu Bhattacharya*[,1]

[1]Microsystems Fabrication Laboratory, [1]Department of Mechanical Engineering, [1]Indian Institute of Technology Kanpur, Kanpur 208016, Uttar Pradesh, India

[2]Department of Electrical and Computer Engineering, University of Missouri Columbia, MO USA

*Corresponding author: bhattacs@iitk.ac.in

Tel- +915122596056; fax- +915122597408

Nanoenergetic materials have been widely explored for obtaining rapid release of energy, burn-speeds and high pressurization rates. In this study, we have synthesized Co_3O_4 nanobelts *via* a simple solid-state process and further integrated as-prepared Co_3O_4 and calcined Co_3O_4 (at 400 ^oC for 4 hr) (Co_3O_4-400) with nano-aluminum (nAl) to realize novel bulk nanoenergetic systems of Co_3O_4/nAl and Co_3O_4-400/nAl respectively. The heat of reaction and combustion performance of these nanoenergetic systems are studied by thermogravimetric and differential scanning calorimetry (TG-DSC), combustion front-wave speed and pressure-time characteristics measurements. The heat of reaction has been measured to be 0.96 kJ g^{-1} for Co_3O_4/nAl and 1.02 kJ g^{-1} for Co_3O_4-400/nAl nanoenergetic systems. The Co_3O_4/nAl nanoenergetic system is able to develop mild peak pressure (12.6±1 to 20±2 MPa) and pressurization rate (0.08±0.05 to 0.14±0.05 MPa/μs) having a characteristics of low gas generation, which can be harnessed in low intensity pressure-pulse based microporation of soft matters like bacterial cells without any lysis. The calcined Co_3O_4 oxidizer is capable to develop more reactive nanoenergetic system than Co_3O_4/nAl, reflecting the generation of moderate peak pressure ((26±2 to 32.6±3 MPa) and pressurization rate (0.29±0.1 to 0.47±0.1MPa/μs). The propagating flames of (Co_3O_4/Co_3O_4-400)/nAl are observed accelerating during instrumented burn tube combustion experiment with front combustion front-wave speed ranging from 480±25 to 830±75 m/s. Through this paper, the Co_3O_4 nanoenergetic oxidizers can be utilized in the generation of low to moderate pressure pulses to transport biological materials to soft matters.

KEYWORDS: cobalt oxide, Al/Co_3O_4, nanothermites, nanoenergetic materials, combustion, metastable intermolecular composites

I. INTRODUCTION

Nanoenergetic materials, a new class of metastable intermolecular composites, comprising nanoscale fuel (aluminum) and oxidizer (CuO, Fe_2O_3, Bi_2O_3, MoO_3 *etc.*) produce rapid release of heat and pressure upon thermite reaction.[1] There are a wide range of possible combinations of metals and oxidizers for energetic material formulations.[2] Aluminum nanopowder is most widely used as fuel in these materials due to its low cost, easy availability and favorable physical properties such as high oxide reducing potential, low vapor pressure, low melting temperature and high thermal conductivity.[3] The nanoscale structuring of oxidizer materials increases their surface area to a wider exposure and reduces the diffusion distances from the close packed fuel particles, thus reducing the atomic length scales of heat and mass transfer between the reactants. This leads to enhancement in both ignition sensitivity and reaction/propagation rate at minimum heat losses.[4] The high speed combustion generating high pressure/shock front-waves found useful applications in microthrusters[5], safe arm and fire devices,[6] drug/gene delivery micro-devices[7] *etc.* Also, it has been widely observed that the energy density and combustion kinetics of nanoenergetic materials are significantly affected by changing the combination of fuel and oxidizer, their nanostructuring and following various preparation/assembling strategies.[8] The most effective nanoenergetic materials can be generated by selection of right fuel-oxidizer combination and their nanostructuring (*viz.*, the shape and size distribution) and assembling at right stoichiometry.

Cobalt oxide (Co_3O_4, p-type semiconductor) has attracted the research community for its wide range of applications in many areas such as electrode materials in rechargeable Li-ion batteries,[9-10] gas sensors[11], catalyst,[12] energy storage,[13] solar energy absorber,[14] magnetic materials,[15] and electronic devices.[16] Owing to its unique physicochemical properties of one dimensional

nanostructures, the various methods such as micro-emulsion-based methods,[17] hydrothermal methods,[18] solvo-thermal methods,[19] co-precipitation/digestion methods,[20] heating cobalt foils in air,[21] sol-gel method[22] *etc*. were developed for the synthesis of Co_3O_4 nanorods,[17-19] nanowires[21] and nanofibers.[22] In this work we have developed Co_3O_4 nanobelts by a simple solid-state method *via* modification of a mechano-chemical method.[23]

In recent years, a rapid growth in design and development of nanoenergetic systems has been observed with scientific and technological advancements in various shape and size metal oxide nanomaterials. Among the various metal oxides, CuO, Bi_2O_3, MoO_3, Fe_2O_3 and WO_3 are widely explored as nanoenergetic oxidizers. The various synthesis methodologies and processing of CuO nanomaterials have developed nanoenergetic composites with moderate to excellent combustion reactivity (combustion front-wave speed and pressurization rate).[24-26] S. Gangopadhayay and groups[24] demonstrated that the CuO/Al nanocomposites were capable to deliver wide-range combustion performance (combustion front-wave speed: 1500 ± 50 to 2400 ± 100 m/s; peak pressure: 22±3 to 70±10 MPa; pressurization rate: 2.5±0.3 to 5.7±0.7 MPa/μs) by adopting various processing methodologies such as vacuum drying and calcination of CuO nanorods at different temperature and time as well as with/without self-assembling the CuO nanorods with aluminum nanoparticles. M. R. Zachariah and groups[25] developed hollow CuO sphere of thin shell thickness using aerosol spray pyrolysis method, which exhibited excellent gas generating and rapid oxygen releasing capabilities, resulting in a high pressurization rate of 0.745 MPa/μs with nanoaluminum combustion. In a similar effort, S. Bhattacharya and groups[26] fabricated super-reactive CuO nanorods by simple biogenic solid-state and sonoemulsion routes utilizing Aloe-vera as green surfactant, which manifested a high combustion performance (average combustion front-wave speed: 620±50 to 1780±75 m/s; maximum peak pressure: 65.4

MPa; maximum pressurization rate: 1.09 MPa/μs) with nanoaluminum combustion. K. S. Martirosyan and groups[27] evaluated the maximum pressure rise of eight nanoenergetic formulations (each of 0.5 g quantity) using commercial grade metal oxides and nanoaluminum in a constant volume (0.342 L) combustion chamber and demonstrated the increasing order of maximum pressure rise (Fe_2O_3/Al < Fe_3O_4/Al < MoO_2/Al < WO_3/Al < MnO_2/Al < MoO_3/Al < CuO/Al < Bi_2O_3/Al) with observation of highest pressure peak of 2.9 MPa with Bi_2O_3/Al. However, when Martirosyan and groups[28] experimented the combustion of nanoenergetic formulation (0.5 g mixture) containing nanoaluminum and combustion synthesized high quality nanocrystalline Bi_2O_3 oxidizer (size: 40-50 nm, wt%: 80%), a very high combustion performance (peak pressure: ~12 MPa; front combustion velocity: ~2500 m/s; pressurization rate: 650 GPa/s) than that of commercial grade Bi_2O_3-based nanoenergetics were achieved. Martirosyan and groups[29] also developed another high reactive nanoenergetic system of Al/I_2O_5, which propagated with a velocity of ~2000 m/s and created a maximum peak pressure of ~11 MPa and pressurization rate of ~2750 GPa/s comparable to (combustion synthesized Bi_2O_3)/Al[28] nanoenergetic system. M. Pantoya and groups[30] ignited the composites I_2O_5/Al and Ag_2O/Al by impact and demonstrated higher average flame propagation rate of 1305±28 m/s with I_2O_5/Al than that of Ag_2O (flame rate of 531±32 m/s). In another investigation of pressurization rate of various metal oxide (CuO/SnO_2/Fe_2O_3/WO_3)/nanoaluminum composites (fixed mass of 25 mg) in a combustion cell (free volume:13 cc) by M R Zachariah and groups,[31] CuO and next SnO_2 were observed creating rapid pressurization rate owing to their high rate of decomposition and release of gaseous oxidizers resulting in pressurization rate in such a descending order of CuO/Al (11.1 Psi/μs), SnO_2/Al (7.7 Psi/μs), Fe_2O_3/Al (0.017 Psi/μs) and WO_3 (0.028 Psi/μs). In an experimental study of the effect of stoichiometry on the combustion behavior of nanoscale

MoO_3/nAl thermite, Dutro *et al.*[32] characterized the propagation velocity and pressure output in a burn tube experiment and reported a steady propagation velocity (~100 to ~1000 m/s) for ~nanoaluminum proportions from 10 to 65 wt% and peak pressures over 8 MPa near stoichiometric compositions.

Cobalt oxide has not been explored as bulk nanoenergetic composites except a recent development in thin-film based nanoenergetic materials onto a silicon substrate.[33] This report[33] talks in details about the formulation of a core-shell structure of Co_3O_4 nanorod coated with aluminum film. Although films deposited in this manner may have a benefit of micro-patterning and may thus possess good integrability with MEMS/nEMS devices still it is always easy to tune the combustion behavior of the bulk nanoenergetic materials. Further bulk materials can be packed in micro-tubes or capillaries to generate high pressurization rate and also shock waves. Their packaging ratio can be easily changed and various oxidizers and tune morphology of the oxidizers can be used in customized applications. In this study, we have synthesized nanoscale Co_3O_4 oxidizer and developed a novel nanoscale energetic composites system with nano-aluminum. We have mathematically estimated the pressure-time characteristics for combustion of our nanoenergetic systems in a pressure-cell chamber based on established gas dynamics model[34], Chapman–Jouguet (CJ) theory.[35] The exploration of this system has been carried out as a basis to create lower pressures and a higher pressurization rate which is very suitable for the application of delivering particles/genes into soft extra-cellular structures of micro-organisms. We have investigated the combustion front-wave speed and peak pressure/ pressurization rates by igniting these composites.

II. Experimental Section

A. Synthesis of Co_3O_4 nanobelts

All chemical reagents used in the synthesis process were of analytical grades and applied without processing. Co_3O_4 nanobelts were synthesized by simple solid-state chemical mixing of $CoCl_2.6H_2O$ (Source: RFCL Ltd, India, Purity: 98%) and sodium bicarbonate (Source: Fisher Scientific, India, Purity: 99%) in presence of water and hexamethylenetetramine (HMTA) (Source: Merck Specialties Pvt Ltd, India, Purity: 99.99 %). In a typical synthesis process, 2.38 g $CoCl_2.6H_2O$ and 2.1 g $NaHCO_3$ were mixed and ground together in presence of 0.280 g HMTA for few minutes in a mortar and pestle. After getting a homogeneous mixture, 2 ml of de-ionized water was added and mixing was carried on up to 20-30 minutes till a pink homogeneous paste was obtained. The pink paste was extracted from the mortar as well as the pestle and washed several times with water and ethanol in order to get pure cobalt oxide precursor. This precursor was observed to be an intermediate step and after heating the paste in an oven for 180 ^oC for 4 hr, black-colored pure Co_3O_4 was obtained.

B. Preparation of nanoscale energetic composites

Nanoenergetic composite of 0.225 g quantity was prepared by homogeneous dispersion of accurately weighed Co_3O_4 oxidizer nanobelts with aluminum nanoparticles in 30 ml of 2-propanol solution using a sonic wand. These materials were further mixed at different equivalence ratios[36] which was calculated after considering the actual active aluminum content in the aluminum nanoparticles by subtracting the aluminum oxide layer. The aluminum nanoparticles utilized in nanoenergetic composites were of spherical shape with average diameter of 80 nm (Source: Neo Ecosystems and Software Private Ltd. India, Purity: 99%). The sonication process promoted a better homogenized mixing of fuel and oxidizer nanostructures and also helped in breaking up agglomerates if any were formulated by coupling sonic waves to

the particulate system. After sonication for about 3-5 minutes, the well homogenized slurry obtained was poured out in a glass petri-dish and dried at 90^{o} C to evaporate out the 2-propanol dispersant media completely. The dried nanoenergetic composites were carefully retrieved by scrapping off very carefully with a pre-cleaned end of spatula and vacuum stored. The retrieval process of the composite is a skillful step as too much pressure of scrapping off may ignite the material and thus standard precautions at this step are advised.

C. Nanomaterials Characterization

The crystal structure and composition of Co_3O_4 nanobelts was determined by powder X-ray diffraction (XRD) analysis using PANalytical X'Pert Pro diffractometer in the 2θ range of 30–80^{o} at scan rate of 0.02 s^{-1} with Cu Kα radiation of wavelength 1.5418 Å. The surface morphology of Co_3O_4 nanobelts was characterized by transmission electron microscopy (TEM) at accelerating voltage of 200 kV using FEI Technai, 20 UT. The surface morphology of aluminum nanoparticles and its nanoenergetic composites with Co_3O_4 nanobelts were characterized by scanning electron microscopy (Supra 40 VP, Zeiss Germany).

Combustion Characterization of nanoenergetic composites were conducted *via* TGDSC measurements, combustion front-wave speed measurements and pressure−time characteristics measurements at different equivalence ratio. The equivalence ratio was evaluated by considering the actual active aluminum content of Al(core)/Al_2O_3(shell) nanoparticles. The equivalence ratio (φ) was calculated by the Eqn. (1), in which *m* refers to the mass of fuel/oxidizer, and the subscripts *act* and *st* imply actual ratio and stoichiometry ratio respectively.

$$\varphi = \frac{(m_{Al}/m_{Co_3O_4})_{act}}{(m_{Al}/m_{Co_3O_4})_{st}} \qquad (1)$$

The thermogravimetric mass changes and the heat of reaction of Co_3O_4 based nanoenergetic composites were experimentally measured by thermogravimetric and differential scanning calorimetric (TG-DSC) analysis conducted on Netzsch STA 449F3 instrument. The TG-DSC analysis was conducted from 50 to 800 ^oC at a heating rate of 10 K min^{-1} under nitrogen gas supply (99.999 % purity).

The combustion front-wave speed was measured by initiating the combustion of 0.225 g of nanoenergetic composites filled in a constant volume polycarbonate burn tube of inside diameter of 3.18 mm and volume of 0.8 cm^3. The nanoenergetic combustion was initiated from either side of the burn tube by Nichrome wire connected to a 9V DC power source. The combustion front-wave propagation was optically detected by four fiber optics (Thor Labs) coupled photo-detectors (Thor Labs, DET 10A/M) placed in-line at inter-fiber distance of 25 mm over the burn tube. The combustion front-wave speed was measured by the estimation of inter-fiber response time recorded in Tektronix oscilloscope DPO 3054 after the successive flame propagation distance of 25 mm from the previous optical fiber position.

The pressure and pressurization rate of nanoenergetic composites was measured by conducting the combustion experiment of 30 mg of Co_3O_4/nAl nanoenergetic composites in a constant volume pressure cell (diameter=6.25 mm, depth= 5 mm). The nanoenergetic composites were loosely filled in the pressure cell with a packing density of 0.2 g cm^{-3}. A piezoelectric based pressure sensor PCB119B12 (PCB Piezotronics) was rigidly fixed to the pressure cell to measure the pressure-time characteristics of nanoenergetic combustion. The pressure-time characteristics output was recorded by Tektronix digital oscilloscope DPO3054. The details of pressure/pressurization rate and combustion front-wave speed measurements can be found in our

previous publication[26] and these measuring set ups are shown in supplementary Fig. S1 and S2 respectively.

III. Results and Discussion

A. Morphology and crystallography. The phase of the as-prepared and calcined nanomaterials was identified by X-ray diffraction (XRD).The X-ray diffractogram of as-prepared and calcined Co_3O_4 (Co_3O_4-400) nanomaterials is shown in Fig. 1. All XRD peaks were compared to the standard powder XRD data files maintained by Joint Committee on Powder Diffraction Standards (JCPDS) and were found to consistent with the card number JCPDS 9-418 of spinel Co_3O_4 cubic structure. No characteristics peak relates to the CoO which demonstrates the formation of pure phase Co_3O_4. The XRD peaks of Co_3O_4-400 nanomaterials were found sharper and of higher intensity than that of Co_3O_4, which demonstrates the higher crystallinity of calcined Co_3O_4 nanomaterials. The morphology and crystallography of as-synthesized Co_3O_4 were determined by TEM and selected area electron diffraction (SAED) analysis. Fig. 2 (a) and (b) represent the TEM image of Co_3O_4 samples and related SAED pattern respectively. The TEM image indicates the formation of nanobelts like structures of Co_3O_4. From the TEM image, the formation of very small nanoparticles of diameters of ~3-5 nm was also observed. It is evident from the SAED ring pattern that the Co_3O_4 sample is polycrystalline in nature. The X-ray diffractogram of Co_3O_4/nAl nanoenergetics clearly indicates the peak of aluminum nanopowder. Fig. 2 (c) shows the FESEM image of aluminum nanoparticles of average diameter of 80 nm with the inset high magnification TEM image of nanoaluminum demonstrating the Al_2O_3 shell thickness of ~4 nm.

B. Fourier Transform Infrared (FTIR) Analysis

The FT-IR Spectrum of Co_3O_4 and Co_3O_4-400 nanocrystals are represented in Fig. 3. The absorption peaks at wave number 3377 and 1624 cm^{-1} of Co_3O_4 and 3435 cm^{-1} and 1632 cm^{-1} of Co_3O_4-400 could be attributed to the (OH) stretching and bending mode respectively due to possible consequence of water adsorptions from the environment and during handling which causes the surface of the Co_3O_4 samples to be hydroxilated. The absorption peak at 1384 cm^{-1} is observed only with Co_3O_4 which may be related to the surface impurity of poly(oxymethylene)glycols, remained even washing several times the Co_3O_4 precipitates with deionized water. HMTA is decomposed in to ammonia and formaldehyde and ammonia supplies hydroxyl ion slowly after further hydrolization with water.[37] The formaldehyde is soluble in the water as it forms a oligomers of poly(oxymethylene)glycols ($HO(CH_2O)_nH$) with water solution.[38] The contents of formaldehyde which become soluble in water in the form of poly(oxymethylene)glycols is expected to be removed but the content of poly(oxymethylene)glycols which form strong surface bonding with the Co_3O_4 nanocrystals remains as an impurity even several times water cleaning. The strong absorption peaks observed at 563 and 660 cm^{-1} of Co_3O_4 and 566 and 660 cm^{-1} of Co_3O_4-400 correspond to the stretching vibrations of metal oxide for tetrahedrally coordinated Co^{+2} metal ions and octahedrally coordinated Co^{+3} metal ions.[39]

C. Possible Formation Mechanism

The solid-state synthesis process in presence of HMTA is able to form nanobelts cum nanoparticles morphology of Co_3O_4 than only nanoparticles[23] morphology in the absence of HMTA which demonstrates the significant role of HMTA for its anisotropic nanobelts structuring of Co_3O_4 in solid phase reaction process. FTIR measurement confirms the presence of HMTA with Co_3O_4 nanocrystals. From the Reaction (2), the nucleation and growth of cobalt

hydroxyl carbonate ($Co_2(OH)_2CO_3$) can be interpreted. The gradual release of hydroxyl ions by HMTA during solid state mixing process may be envisioned to transit the occurrence of reaction process in comparatively higher basic media which furnishes the stable anisotropic growth of cobalt hydroxyl carbonate nanocrystals. HMTA has been demonstrated to have greater affinity with a particular facet of Co^{+2} nuclei, hence selectively absorbs to this facet depending on the ratio of Co^{+2} and HMTA.[40] In a similar way, the HMTA is proposed to absorb selectively on to the particular facet of cobalt hydroxyl carbonate and minimizes the energy of this facet. Thus the high energy facets of cobalt hydroxyl carbonate experience higher driving force of crystal growth resulting in anisotropic formulation of nanobelt-like structure of cobalt hydroxyl carbonate. Owing to less homogeneity of solid state mixing than solution phase reactions, some cobalt hydroxyl carbonate nanocrystals may not experience favorable condition for nanobelts formulations and thus remains in the form of nanoparticles. The cobalt hydroxyl carbonate nanocrystals are transformed in to Co_3O_4 nanobelts cum nanoparticles when heated at 180 ^oC in oven according to the Reaction (3).

$$2CoCl_2.6H_2O + 4\ NaHCO_3 \longrightarrow 4NaCl + Co_2(OH)_2CO_3 + 3CO_2 + 13H_2O \text{ ----------(2)}$$

$$3Co_2(OH)_2CO_3 + O_2 \longrightarrow 2Co_3O_4 + 3CO_2 + 3H_2O \text{ ---------- (3)}$$

D. Thermogravimetric and Differential Scanning Calorimetry (TGDSC) Measurement

TGDSC measurements were conducted for Co_3O_4/nAl and Co_3O_4-400/nAl nanoenergetic composites at equivalence ratio of 1.6. From thermogravimetric analysis of nanoenergetics as shown in Fig. 4, the weight-loss up to 400 ^oC was found to be greater with Co_3O_4/nAl (4%) than the Co_3O_4-400/Al (1.56 %). The excess weight-loss of 2.44% can be assigned to the surface impurity of oligomers of poly(oxymethylene)-glycols ($HO(CH_2O)_nH$) adhered tightly with

Co_3O_4 nanobelts. In DSC studies, The exothermic peaks were observed at 606 ^oC (onset temperature of 536 ^oC, heat of reaction of 960 J g^{-1}) for Co_3O_4/nAl and at 601 ^oC (onset temperature of 534 ^oC, heat of reaction of 1020 J g^{-1}) for Co_3O_4-400/Al. The higher heat of reaction associated with Co_3O_4-400/nAl may be attributed to its higher pure-phase Co_3O_4-400 oxidizer than Co_3O_4. It may be believed that the higher purity of oxidizer enhances the inter-atomic diffusion reaction with aluminum by releasing oxygen at relatively faster rate. A minor exothermic peak having heat of reaction of 95 J g^{-1} was observed at 424 ^oC for Co_3O_4-400/Al which may be attributed to low temperature redox reactions or interfacial Al−Co−O recrystallization. The exothermic heat of reaction of of Co_3O_4 based nanoenergetics was observed greater than that of PEG400 synthesized CuO nanorods based nanoenergetics (heat of reaction of 850 J g^{-1}) as reported in our earlier publication.[26] The heat of reaction (1.02 kJ/g) of our bulk nanoenergetic system was found ~3.56 times lower than the total heat of reaction of core(Co_3O_4)/shell(Al)[33] nanoenergetic materials prepared on silicon substrate. Core-shell nanostructuring of fuel and oxidizer can be envisaged to enhance the nanoscale intimacy, interfacial contact area as well as purity. Thus, core-shell nanoenergetic can be envisioned to possess higher reactivity due to decreased inter-atomic diffusion path and increased population of fuel and oxidizer atoms per unit surface-area at any instance during exothermic reaction, which can be attributed to higher heat of reaction of core-shell (Co_3O_4/Al) nanoenergetic materials as compared to ultrasonically mixed bulk nanoenergetics. Further, the core-shell (Co_3O_4/Al) thermites, owing to oxidation of aluminum in Ar-O_2 plasma, were examined to possess higher heat of reaction than core(CuO)/Al(shell)[41] thermites. Thus in a nutshell, the higher reactivity and aluminum oxidation in Ar-O_2 plasma of core/shell (Co_3O_4/Al) thermite can be attributed for its higher heat of reaction than our bulk nanoenergetic system.

E. Theoretical Estimation of Pressure Time Characteristics

The pressure-time characteristics of low gas generating Co_3O_4/nAl nanoenergetic composites (mass: 0.03 g) were theoretically estimated and validated by following the gas dynamic model[34] which has been proposed for high reactive mass (0.5 g) combustion of high gas generating Al/Bi_2O_3 in a large volume cylindrical chamber. Even though the gas generation with Co_3O_4/nAl nanoenergetic composites is much smaller than the Bi_2O_3/Al, [27-28, 42] the pressurization rate in our pressure cell (diameter=6.25 mm, depth= 5 mm, Supplementary Fig. S1) can be assumed to be developed at high level and so considered to be consistent to gas dynamic model because of low volume of 0.1534 cm^3 of our pressure-cell as compared to 85.13 cm^3 applied in gas dynamic model.[34] In the model, the energy of solid fuels-oxidizers thermite reaction is released instantly and transferred to the gaseous products. The big explosion based gas dynamic model[34] assumes the generation and propagation of one-dimensional shock wave in the air-filled cylindrical pressure-cell. The heat transfer is considered to be adiabatic and the pressure of the shock wave is assumed to be much greater than the ambient pressure. In big explosion model,[34] the explosion happens very quickly releasing all the explosion energy into the gas instantly before the shock-wave leaves the narrow expansion region and a strong discontinuity condition arises because of the higher pressure magnitude behind the shock wave than the gaseous medium pressure where it is expanding. The Chapman–Jouguet (CJ) theory also assumes the reaction in the shock to be completed instantaneously at the continuum level[35] and based on this CJ theory equation of state for CuO/Al nanothermites have been developed earlier.[43]

The gas dynamic model[34] utilizes the conservation of momentum, entropy and mass to arrive the pressure equation. For theoretical modeling of thermite reaction, we considered the mass of

nanoenergetics to be 30 mg. Following reaction was used to calculate the amount of the Al that would undergo combustion for the given amount of oxidizer.

$$8Al + 3\ Co_3O_4 \longrightarrow 4\ Al_2O_3 + 9\ Co \qquad (4)$$

It was kept in mind that about 20% of nano-aluminum is in the form of Al_2O_3 initially which was calculated for aluminum nanoparticles of average particle size of 80 nm possessing outer shell thickness of Al_2O_3 of ~4 nm determined from high magnification TEM image as shown by inset of Fig. 2 (c). Hence, the actual amount of nanoenergetics after the exclusion of non-reactive Al_2O_3 was calculated for equivalent ratio of 1.6 which is summarized in supplementary Table S1. It is assumed that the outer shell of Al *i.e.* Al_2O_3 acts as heat sink thus the various level of its contents in different equivalent ratio of nanoenergetics modify the combustion pressure.

The experimental module that is developed for the testing of the nanoenergetic composite materials is a constant volume pressure cell fully packaged with the composite materials. The pressure sensor used to measure the pressurization rate and peak pressure in our experiments have been positioned at the end of the pressure-cell and is supposed to measure the total force acting on it per unit area which is a function of both the incoming pressure and the drag force and its value depends heavily on the orientation of the detector.[25] The pressure sensor normally does not feel any drag force i.e., drag coefficient (γ) =0, if it is placed along the combustion propagation direction in the chamber. If it is assembled perpendicular to the drag force, the effect of drag is maximum and the drag coefficient is assumed to be 2 in that situation. In our experiments the pressure sensor is placed perpendicular to the direction of propagation of the pressure wave although due to relatively very less pressure-cell volume and fast pressurization rate, the drag to combustion propagation is insignificant and we assume the value of (γ) =0 for

all our calculations. A theoretical big explosion gas dynamic model was utilized based on the the following equations[25] of combustion pressure.

$$P + \frac{1}{2}\gamma\rho v^2 = \left(\frac{4L^2\rho_1}{9t^2}\right)\left(\frac{1}{\gamma}DZ + \frac{1}{2}\gamma DV^2\right) \quad (5)$$

Where, $\mathcal{V} \equiv \mathcal{V}(\xi[t]), \xi[t] = \left(\frac{\rho_1 L^3 A}{Et^2\beta^3}\right)^{\frac{1}{3}}$, Here P, ρ and v are the gas pressure, gas density and gas velocity respectively. L and A is the length and cross-section area of the cylindrical pressure-cell chamber. The symbol ρ_1 refers to the gas density in front of propagating shock wave whereas β and ξ to a dimensionless constant and dimensionless variable. Eqn. (6) is used to calculate the magnitude of ξ. E is the energy released during the exothermic reaction. $\mathcal{V}(\xi)$ represents a function inverse to the function $\xi(V)$. Due to the complexity of the equation below, an indirect approach was used to solve it. The limits of $\mathcal{V}$ vary from 1/γ to 2/γ+1 (from ξ=0 to ξ=1) and the iterations are performed in MATLAB. D and Z are the dimensionless function and can be estimated by the Eqn. (7) and (8) respectively.

$$\xi^3 = \frac{4\left(\frac{\gamma+1}{\gamma-1}(\gamma\mathcal{V}-1)\right)^{\frac{3(\gamma-1)}{2\gamma-1}}(3-(1+\gamma)\mathcal{V})^{-\frac{5\gamma-4}{2\gamma-1}}}{(1+\gamma)^2\mathcal{V}^2} \quad (6)$$

$$D = \frac{\gamma+1}{\gamma-1}\left(\frac{\gamma+1}{\gamma-1}(1-\mathcal{V})\right)^{\frac{-2}{2-\gamma}}\left(\frac{\gamma+1}{\gamma-1}(\gamma\mathcal{V}-1)\right)^{\frac{1}{2\gamma-1}} \times (3-(1+\gamma)\mathcal{V})^{\frac{-(5\gamma-4)}{(\gamma-2)(2\gamma-1)}} \quad (7)$$

$$Z = -\frac{\gamma(\gamma-1)\mathcal{V}^2(\mathcal{V}-1)}{2(\gamma\mathcal{V}-1)} \quad (8)$$

The value of β was considered to be 1.229 for γ=1.4. Following these equations,the pressure *v/s* time characteristics wasobtained for all the three equivalent ratios assuming the drag coefficient to be zero.

The pressure curve is calculated by solving equations 5 through 8. MATLAB8.2 is used for calculating the peak pressure and also the pressurization rate. Fig. 5 (a) and (b) show the plot of estimated gas pressure (in MPa) with respect to time (microseconds) corresponding to an equivalence ratios 1.6 for Co_3O_4/nAl and Co_3O_4-400/nAl respectively. The peak pressure was estimated to be 25.35 MPa and 36.95 MPa respectively for Co_3O_4/nAl and Co_3O_4-400/nAl.

E. Combustion Performance of Co_3O_4/nAl and Co_3O_4-400/nAl nanoenergetic composites

Combustion front-wave speed, peak pressure and pressurization rate measurement of Co_3O_4/nAl at equivalence ratio of 1.4, 1.6 and 1.8 has been shown in supplementary Table S2. The pressure-time characteristics curve of Co_3O_4/nAl and Co_3O_4-400/nAl as a function of equivalence ratio has been drawn and shown in Fig 5 (c) and (d).The peak pressure and pressurization rate of Co_3O_4/nAl and Co_3O_4-400/nAl were measured maximum at equivalence ratio of 1.6 developing peak pressure of 20±2 MPa (Pressurization rate=0.14±0.03 MPa/μs) and 32.6±3 MPa (Pressurization rate=0.47±0.1MPa/μs) respectively. The peak pressure so measured rhymes well with the theoretically predicted value although as estimated earlier the pressurization rate is not so huge. The time scale of experimental pressure-time characteristics (pressurization rate) is in fact ~100 times more than that predicted theoretically due to diffusional restrictions. In reality, the exothermic reactivity of nanoenergetic formulation and henceforth the gas release rate during combustion depends on the population of fuel and oxidizer atoms in contact and inter-atomic diffusion path which will disallow the pressure wave to travel such a super high rate as predicted

in theoretical estimation. The pressure rise time of cobalt oxide based nanoenergetics is measured to be 70 μs (Co_3O_4-400/nAl at φ=1.6), which is seven times higher than that of our Bi_2O_3/Al[42] based nanoenergetic films. The shorter time scale of Bi_2O_3/Al[42] nanoenergetic films than Co_3O_4-400/nAl can be attributed to its higher gas generating ability and less diffusional restriction owing to core-shell nanostructuring. Thus, we may conclude that the time scale of cobalt oxide based nanoenergetics can be shortened and approached towards theoretical one by nanotechnological efforts (Fabrication of high-aspect, high purity Co_3O_4 nanostructures and their molecular level as well as stoichiometric assembling with nanoaluminum).

The pressure-time characteristics achieved with Co_3O_4-400/nAl was found better than the PEG synthesized CuO nanorods (CuO_{peg}) based nanoenergetics (Peak Pressure=27.4±2 MPa, Pressurization rate=0.25±0.1 MPa/μs) as reported in our previous findings.[26] In another pressure-time characteristics experiment,[24] the commercial grade CuO based nanoenergetics developed lowest peak pressure and pressurization rate of magnitude 22±3 MPa and 2.5±0.3 MPa/μs respectively among their all kinds of CuO oxidizers of packing density of 0.33 g/cm^3. Thus the low pressure-time characteristics of Co_3O_4/nAl really helps us to achieve a softer system of delivery of a pressure waves which would not cause much damage to the soft cellular system as has eventually been the goal behind all the material synthesis reported in this work. The peak pressure (32.6±3 MPa) of calcined Co_3O_4 based nanoenergetics is comparable to that of CuO nanoparticles (calcined at 400 ^oC for 3 h of CuO-100 nanorods) based nanoenergetics (Peak Pressure=35±3 MPa). The considerably lower pressurization rate of Co_3O_4-400/nAl than the CuO nanoparticles (calcined at 400 ^oC for 3 h of CuO-100 nanorods) based nanoenergtics[24] can be attributed to its lower theoretical gas generations[2]. Theoretical gas release of Co_3O_4/nAl nanoenergetic composites is about 62 % lesser than the gas release with the CuO/nAl

nanoenergetic composites. The combustion behavior of Co_3O_4/nAl nanoenergetics at equivalence ratio of 1.8 is observed to be anomalous giving highest combustion velocity but developing smallest pressurization rate. It can be hypothesized that, since the combustion front-wave propagation distance in pressure cell is much shorter (i.e. 5 mm) than that in burn-tube experiment (i.e. 100 mm), therefore the higher thermal conductivity of nanoenergetics associated with equivalence ratio of 1.8 may not contribute much in pressurizing the combustion front-waves. The higher available oxygen atoms at equivalence ratio of 1.6 can be believed to increase the exothermic reaction and thus the pressurization rate.

The combustion front-wave speed (correspond to speed between photo-detectors 3 and 4) of Co_3O_4/nAl and Co_3O_4-400/nAl nanoenergetics at different equivalence ratios can be seen in Fig. 6. From the inset photo-detector output *vs* time plot of Fig. 6, the interval time between two photo-detectors is observed decreasing in forward direction, which implies that the combustion wave-front accelerates in forward direction in confined burn tube. It can be envisioned that the pressure build-up due to high combustion/exothermic reactivity and gas generation in confined burn tube during combustion process propel the flame front propagation at a faster rate in forward direction. The pressure build up may also hypothesized to enhance the ignition sensitivity of nanoenergetic composites lying ahead of the flame front and therefore the ignition of nanoenergetic composites happens at early stage of time in forward direction. Thus, the accelerating rate of combustion flame-front speed may be believed to depend on the intensity of pressure-build up, forward pressure wave speed and the rate of confinement of burn tube. However, it can further be envisaged that the pressure wave would accelerate the combustion flame front propagation only, if it is travelling at a higher speed than the combustion flame front speed. The combustion front-wave speed of calcined Co_3O_4 based nanoenergetic composites

was found to be maximum at equivalence ratio of 1.6 where as for Co_3O_4/Al nanoenergetics, an increasing trend in combustion front-wave speed with equivalence ratio can be observed. It can be interpreted that the presence of surface impurity of poly(oxymethylene)glycols to the uncalcined Co_3O_4 may require excess aluminum than that of calcined Co_3O_4 oxidizer which may be the reason of developing higher combustion front-wave speed at equivalence ratio of 1.8 in Co_3O_4/nAl nanoenergetics. It is also observed from combustion front-wave speed plot that there is lower deviation in combustion front-wave speed in between equivalence ratio of 1.6 to 1.8 than that between 1.4 to 1.6 which can be explained by considering the higher thermal conductivity of nanoenergetic composites due to increase in the relative quantity of nano-aluminum at higher equivalence ratio. The higher thermal conductivity can be believed to create a faster hot spot at the front of combustion front-wave which may accelerate the combustion front-wave propagation along the total travel of 100 mm in the burn-tube experiment.

IV. Conclusions

In summary, nanoscale Co_3O_4 consisting of small nanoparticles (diameter ~3-5 nm) and nanobelts (diameter of 5-10 nm, lengths of up to 100 nm) were synthesized by a simple solid-state method and were characterized by XRD, TEM, SAED and FTIR. The nanoscale Co_3O_4 was utilized as oxidizer in developing novel bulk nanoenergetic composites with nanoaluminum. The calcined Co_3O_4 based nanoenergetic composites *i.e.* Co_3O_4-400/nAl exhibited better exothermic heat of reaction and combustion performance than that of uncalcined one. Based on TGDSC measured heat of reaction and pressure-cell design parameters, the peak pressure and pressurization rate were theoretically estimated and when compared to the experimentally measured pressure-time characteristics, a good agreement between predicted peak pressure and measured peak pressure was found. The Co_3O_4/nAl and Co_3O_4-400/nAl nanoenergetics were

able to propagate at a maximum flame-front speed of 781±50 and 830±75 m s^{-1} respectively. These nanoenergetic systems are able to develop peak pressure ranging from mild (12.6±1 to 20±2 MPa with Co_3O_4/nAl) to moderate (26±2 to 32.6±3 MPa with Co_3O_4-400/nAl) during combustion experiment inside a constant-volume pressure cell experiment with charge density of 0.2 g cm^{-3}. The maximum peak pressure was obtained at equivalence ratio of 1.6 and was nearly comparable to the CuO based nanoenergetic system but the maximum pressurization rate with Co_3O_4/nAl (0.47±0.1MPa/μs) was much below to that of CuO/nAl nanoenergetics owing to low gas generation during combustion process. The heat of reaction was measured to be 0.96 kJ g^{-1} for Co_3O_4/nAl and 1.02 kJ g^{-1} being greater to that of PEG400 synthesized CuO nanorods based nanoenergetics. Through this work we report a new set of nanoenergetic composite that can be used for creating mild to moderate pressure waves.

Supporting Information

The pressure-time characteristics measuring set-up and combustion front-wave speed measuring set-up have been shown in supplementary Fig. S1 and S2. Reactive mass distribution and Combustion (front-wave speed and pressure-time) measurements of nanoenergetic composites have been listed in supplementary Table S1 and S2 respectively.

Acknowledgements

The authors sincerely thank to Science Engineering and Research Council, Department of Science and Technology, Government of India for its financial support. The author would also like to acknowledge Nanoscience Center and Department of Materials Science and Engineering of Indian Institute of Technology Kanpur for providing good material characterization facilities.

References

1 C. E. Aumann, G. L. Skofronick and J. A. Martin, *J. Vac. Sci. Technol. B: Microelectron. Nanometer Struct. Process., Meas., Phenom.,* 1995, **13**, 1178−1183.

2 S. H. Fischer and M. C. Grubelich, Proceedings of 24th International Pyrotechnics Seminar, Monterey, CA, 1998, 231−286 (also a Sandia Technical Report, No. SAND98-1176C).

3 C. Rossi, K. Zhang, D. Esteve, P. Alphonse, P. Tailhades and C. Vahlas, *J. Microelectromech. Syst.,* 2007, **16**, 919−931.

4 S. F. Son, B. W. Asay, T. J Foley. R. A. Yetter, M. H. Wu, and G. A. Risha, *J. Propul. Power,* 2007, **23**, 715−721.

5 S. J. Apperson, A. V Bezmelnitsyn, R. Thiruvengadathan, K. Gangopadhyay, S. Gangopadhyay, W. A. Balas, P. Anderson and S. M. Nicolich, *J. Propul. Power,* 2009, **25**, 1086−1091.

6 H. Pezous, C. Rossi, M.Sanchez, F. Mathieu, X. Dollat,; S. Charlot, L. Salvagnac and V. Conedera, *Sens. Actuators, A,* 2010, **159**, 157−167.

7 M. Korampally, S. J Apperson, C. S. Staley, J. A. Castorena, R. Thiruvengadathan, K. Gangopadhyay, R. R. Mohan, A. Ghosh, L. Polo-Parada and S. Gangopadhyay, *Sens. Actuators, B,* 2012, **171−172**, 1292−1296.

8 X. Zhou, M. Torabi, J. Lu, R. Shen and K. Zhang, *ACS Appl. Mater. Interfaces*, 2014, **6**, 3058-3074.

9 B. Guo, C. S. Li, and Z. Y. Yuan, *J. Phys. Chem. C*, 2010, **114**, 12805-12817.

10 X. W. Lou, D. Deng, J. Y. Lee, J. Feng and L. A. Archer, *Adv. Mater.,* 2008, **20**, 258–262.

11 W. Y. Li, L. N. Xu and J. Chen, *Adv. Funct. Mater.,* 2005, **15**, 851-857.

12 J. Jansson, A. E. C. Palmqvist, E. Fridell, M. Skoglundh, L. Österlund, P. Thormahlen and V. Langer, *J. Catal.* 2002, **211**, 387−397.

13 J. Ryu, S.-W. Kim, K. Kang and C. B. Park, *ACS Nano*, 2009, **4**, 159 –164.

14 E. Barrera, T. Viveros, A. Montoya and M. Ruiz, *J. Sol. Energy Mater. Sol. Cells,* 1999, **57**, 127-140.

15 S. A. Makhlouf, *J. Magn. Magn. Mater.* 2002, **246**,184-190.

16 L. Fu, Z. Liu, Y. Liu, B. Han, P. Hu, L. Cao and D. Zhu, *Adv. Mater.,* 2005, **17**, 217−221.

17 R. Xu, J. W. Wang, Q. Y. Li, G. Y. Sun, E. B. Wang, S. H. Li, J. M. Gu and M. L. Ju, *J. Solid State Chem.,* 2009, **182**, 3177–3182.

18 F. Teng, M. Chen, G. Li, Y. Teng, T. Xu, Y. Hang and Y. Zhu, *Appl. Catal., B* 2011, **110**, 133–140.

19 S. Lian, E. Wang, L. Gao and L. Xu, *Mater. Lett.,* 2007, **61***,* 3893-3896.

20 D. Patil, P. Patil, V. Subramanian, P. A. Joy and H. S. Potdar, *Talanta*, 2010, **81**, 37-43.

21 Z. Dong, Y. Fu, Q. Han, Y. Xu, and H. Zhang, *J. Phys. Chem. C*, 2007*,* **111**, 18475-18478.

22 B. B. Lakshmi, C. J. Patrissi, and C. R. Martin, *Chem. Mater.*, 1997, **9**, 2544-2550.

23 H. Yang, Y. Hu, X. Zhang and G. Qiu, *Mater. Lett.,* 2004, **58**, 387-389.

24 R. Thiruvengadathan, A. Bezmelnitsyn, S. Apperson, C. Staley, P. Redner, W. Balas, S. Nicolich, D. Kapoor K. Gangopadhyaya and S. Gangopadhyaya, *Combust. Flame,* 2011, **158**, 964−978.

25 G. Jian, L. Liu and M. R. Zachariah, *Adv. Funct. Mater.,* 2013, **23**, 1341−1346.

26 V. K. Patel and S. Bhattacharya, *ACS Appl. Mater. Interfaces*, 2013, **5**, 13364-13374.

27 K. S. Martirosyan, L. Wang, A. Vicent and D. Luss, *Propellants Explos. Pyrotech.*, 2009, **34**, 532 – 538.

28 K. S. Martirosyan, L. Wang, A. Vicent and D. Luss, *Nanotechnology*, 2009, **20,** 405609.

29 K. S. Martirosyan, L. Wang and D. Luss, *Chem. Phys. Lett.*, 2009, **483**, 107–110.

30 R. Russell, S. Bless and M. Pantoya, *J. Energ. Mater.*, 2011, **29**, 175-192.

31 K. Sullivan and M R Zachariah, *J. Propul. Power*, 2010, **26**, 467-472.

32 G.M. Dutro, R.A. Yetter, G.A. Risha and S.F. Son, *Proc. Combust. Inst.*, 2009, **32**, 1921–1928.

33 D. Xu, Y. Yang, H. Cheng, Y. Y. Li and K. Zhang, *Combust. Flame,* 2012, **159**, 2202−2209.

34 K. S. Martirosyan, M. Zyskin, C. M. Jenkins and Y. Horie, *J. Appl. Phys.,* 2012, **112**, 094319.

35 W. Fickett and W. C. Davis, *Detonation;* University of California Press: Berkeley, **1979**.

36 K. B. Plantier, M. L. Pantoya and A. E. Gash, *Combust. Flame,* 2005, **140**, 299−309.

37 K. Govender, D. S. Boyle, P. B. Kenway and P. O'Brien, *J. Mater. Chem*., 2004, **14**, 2575-2591.

38 T. Grutzner and H. Hasse, *J. Chem. Eng. Data,* 2004, **49**, 642-646.

39 M. Herrero, P. Benito, F. M. Labajos and V. Rives, *Catal. Today*, 2007, **128**, 129–137.

40 H. Liang, J. M. Raitano, L. Zhang and S.-W. Chan, *Chem. Commun.*, 2009, **48**, 7569–7571.

41 K. Zhang, C. Rossi and G. A. A. Rodriguez, *Appl. Phys. Lett*., 2007, **91,** 113117.

42 V. K. Patel, A. Ganguli, R. Kant and S. Bhattacharya, *RSC Adv.*, 2015, **5**, 14967–14973.

43 Y. Gan, Z. Chen, K. Gangopadhayay, A. Bezmelnitsyn and S. Gangopadhayay. *J Nanopart. Res.,* 2010, **12**, 719–726.

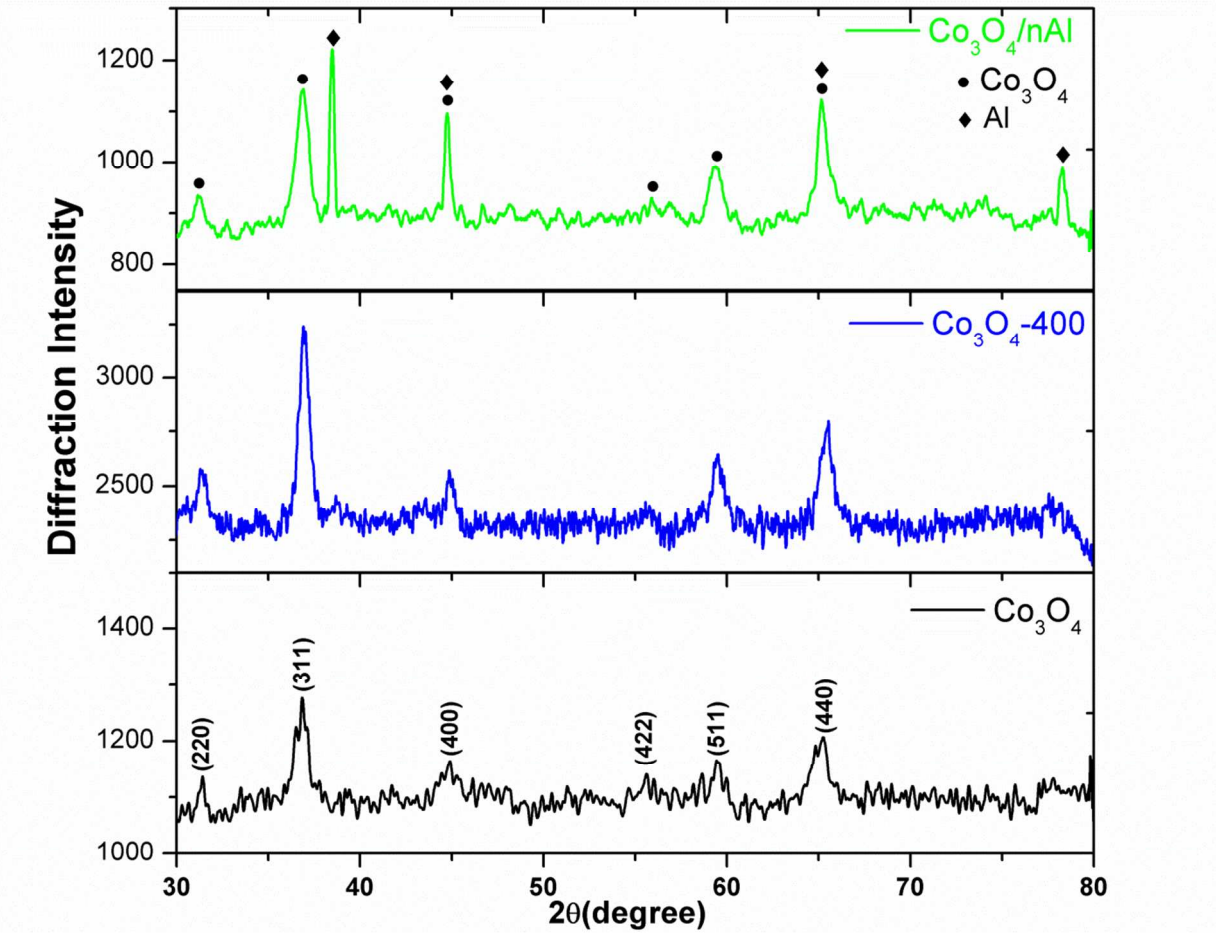

541

542 **Fig 1.** Powder X-ray diffraction pattern of Co_3O_4 (indicated in black), Co_3O_4-400 (indicated in

543 blue) and Co_3O_4/Al nanoenergetics prepared at equivalence ratio of 1.6 (indicated in green)

544

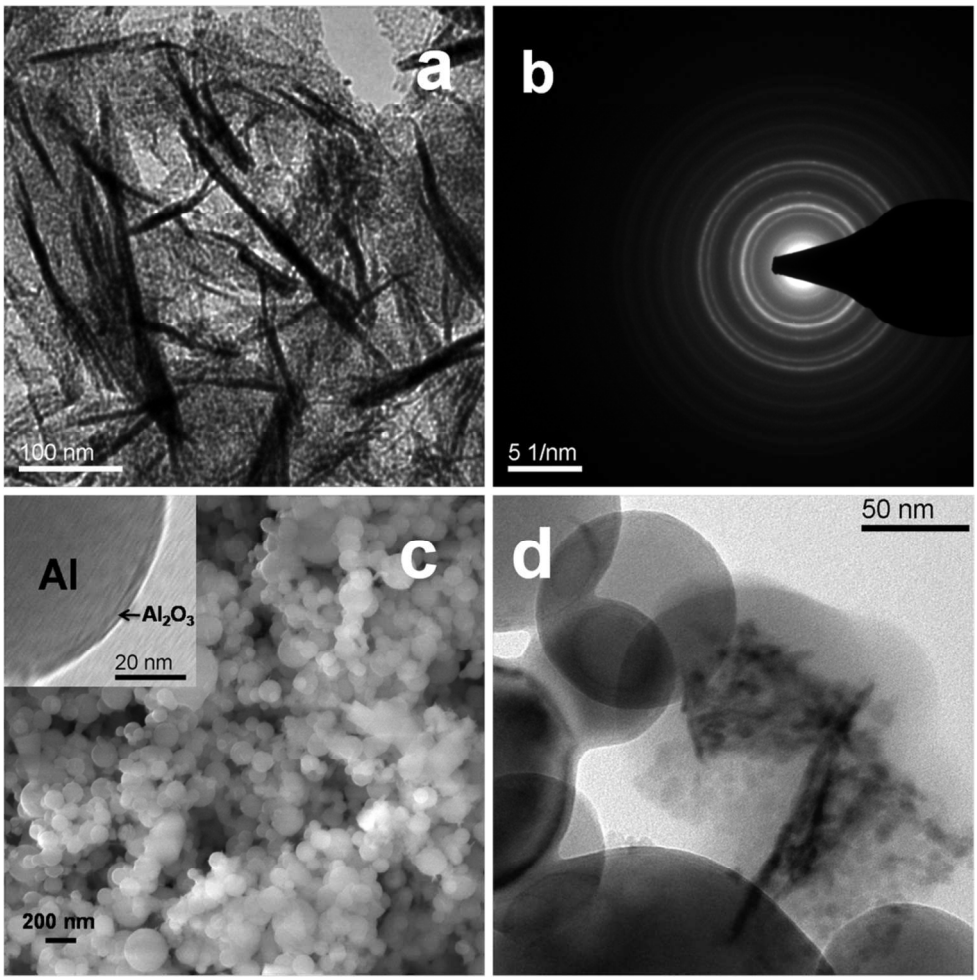

Fig 2. (a) TEM image of Co_3O_4 nanobelts (b) SAED ring pattern of Co_3O_4 nanobelts (c) FESEM image of aluminum nanoparticles with inset of its high magnification TEM image showing the core (Al) and shell (Al_2O_3) (d) TEM image of Co_3O_4/nAl nanoenergetic composites

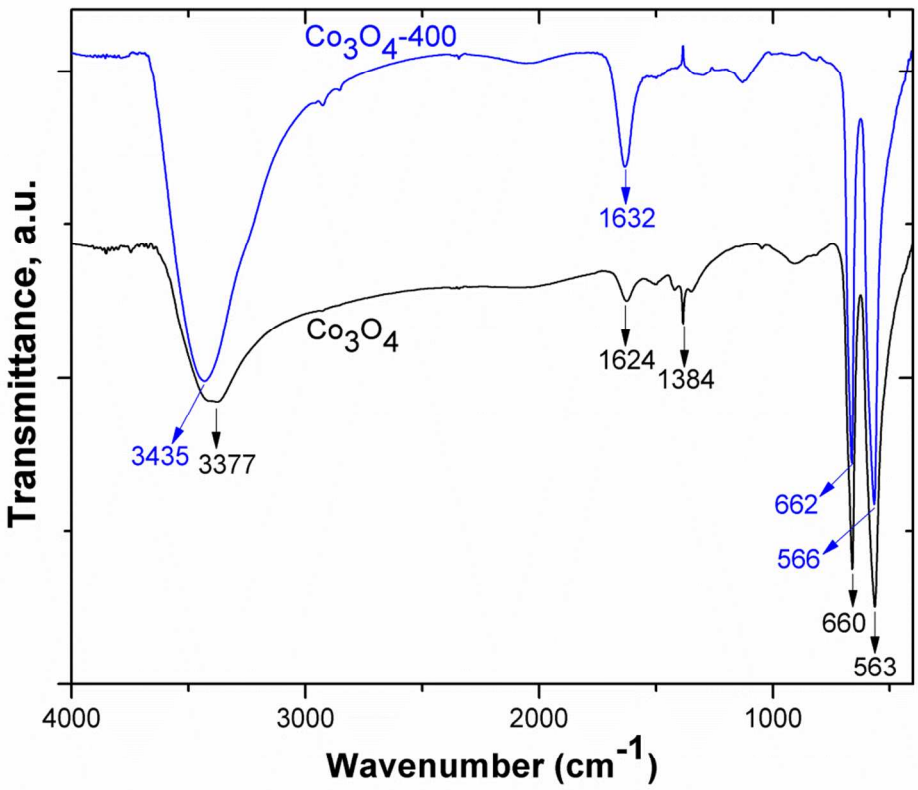

553

554 **Fig. 3** FT-IR Spectrum of Co_3O_4 (indicated in black) and Co_3O_4-400 (indicated in blue)

555 nanomaterials.

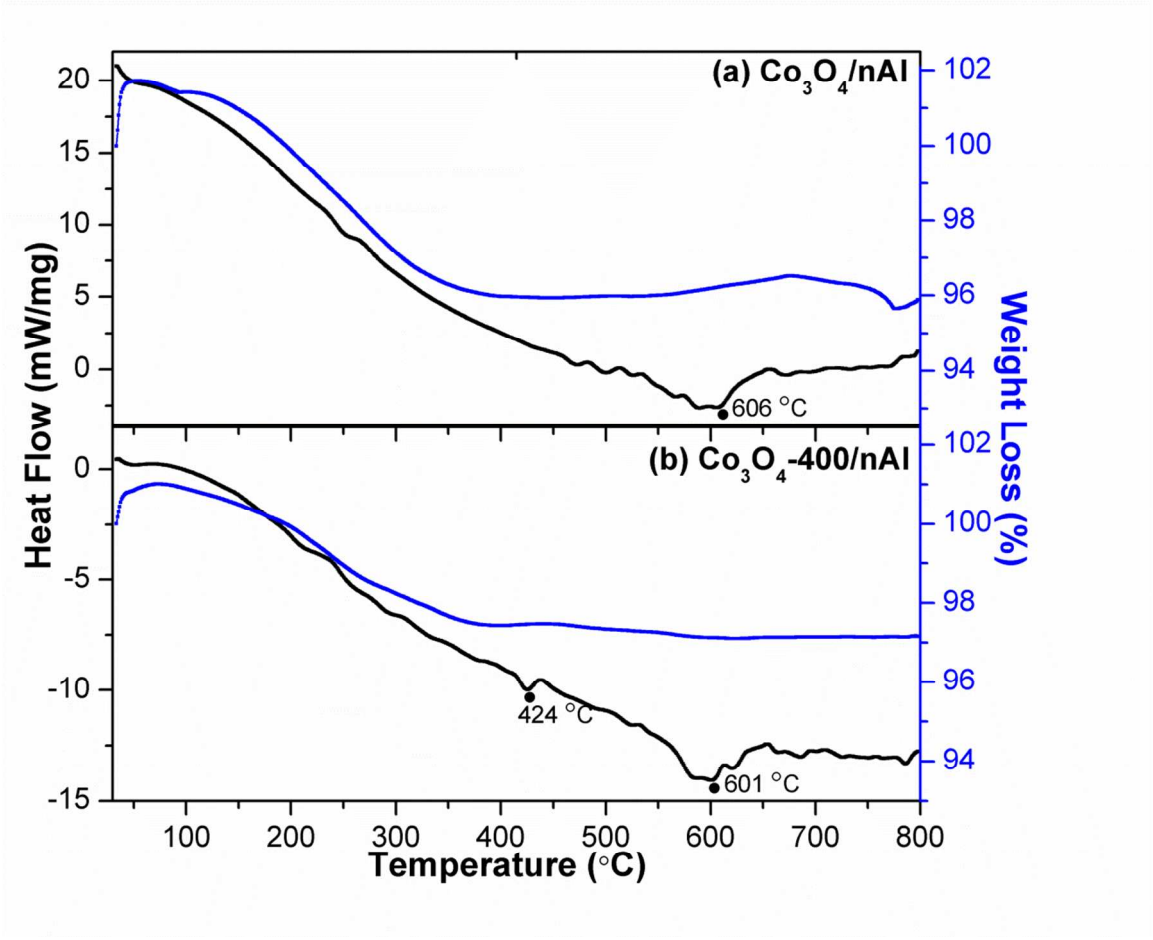

Fig 4. TG-DSC measurements of (a) Co_3O_4/nAl and (b) Co_3O_4-400/nAl nanoenergetics at equivalence ratio of 1.6.

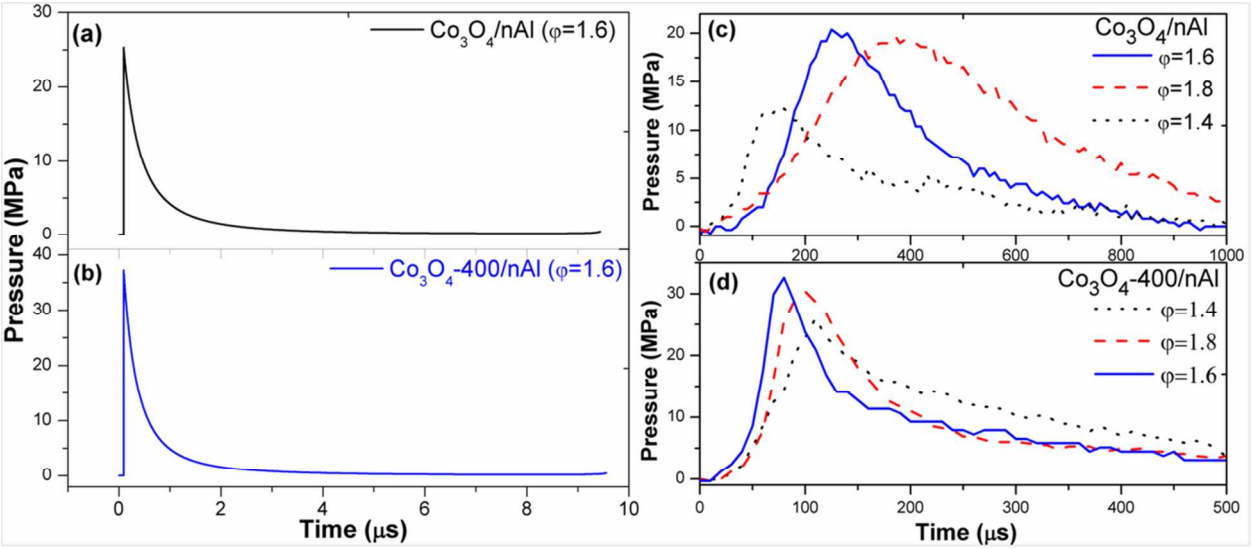

559

560 **Fig. 5** Theoretical Pressure-time characteristics results using MATLAB modeling of big

561 explosion gas dynamic model at equivalence ratios of 1.6 for (a) Co_3O_4/nAl and (b) Co_3O_4-

562 400/nAl, and experimental Pressure−time characteristics of (c) Co_3O_4/nAl (d) Co_3O_4-400/nAl at

563 different equivalence ratio.

564

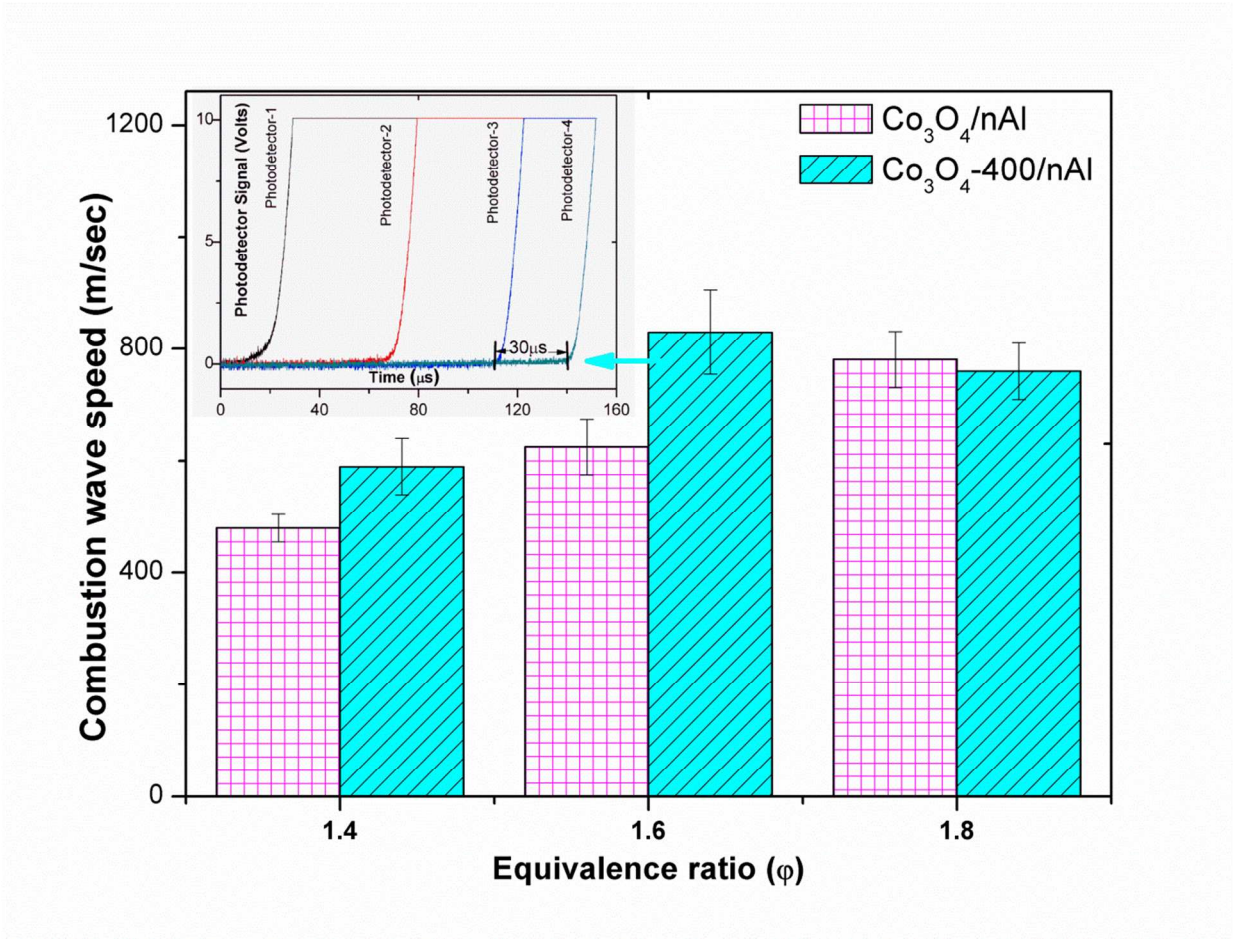

565

566 **Fig 6.** Combustion front-wave speed measurements of Co_3O_4/nAl and Co_3O_4-400/nAl as a

567 function of equivalence ratio with inset plot of photo-detector output vs time.

568

569

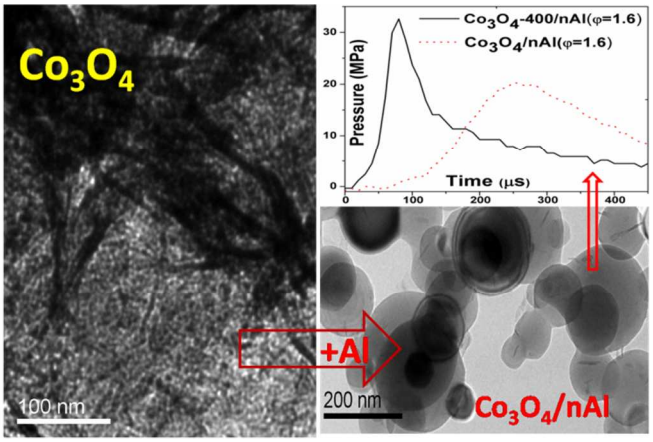

570

571 Novel Co_3O_4 nanobelts based bulk nanoenergetic systems have been developed which are able to
572 generate mild to moderate peak pressure and pressurization rates as demanded in shock wave
573 mediated biomedical applications.

574